Temperature dependency of the toughening capability of electrospun PA66 nanofibers for carbon/epoxy laminates

Saeedifar, Milad; Saghafi, Hamed; Mohammadi, Reza; Zarouchas, Dimitrios

DOI
10.1016/j.compscitech.2021.109061

Publication date
2021

Document Version
Final published version

Published in
Composites Science and Technology

Composites Science and Technology 216 (2021) 109061

Contents lists available at ScienceDirect

Composites Science and Technology

journal homepage: www.elsevier.com/locate/compscitech

Temperature dependency of the toughening capability of electrospun PA66 nanofibers for carbon/epoxy laminates

Milad Saeedifar [a,*], Hamed Saghafi [b,c], Reza Mohammadi [d], Dimitrios Zarouchas [a]

[a] Structural Integrity & Composites Group, Faculty of Aerospace Engineering, Delft University of Technology, Delft, the Netherlands
[b] Department of Mechanical Engineering, Tafresh University, Tafresh, Iran
[c] New Technologies Research Center (NTRC), Amirkabir University of Technology, Tehran, Iran
[d] Non-destructive Testing Lab, Department of Mechanical Engineering, Amirkabir University of Technology, Tehran, Iran

ARTICLE INFO

Keywords:
Nano composites
Fracture toughness
Fractography
Scanning electron microscopy
Electro-spinning

ABSTRACT

The present study evaluates the toughening capability of electrospun PA66 nanofibers for carbon/epoxy composite laminates subjected to mode II loading conditions at elevated temperatures. The Dynamic Mechanical Analysis (DMA) test showed that the glass transition temperature of the produced nanofibers is in a range of ~60–80 °C. Accordingly, End-Notched Flexure (ENF) carbon/epoxy specimens interleaved by a 50 μm-layer of electrospun PA66 nanofibers were subjected to the quasi-static mode II loading at room temperature (~25 °C), 100 °C, 125 °C, and 160 °C. At room temperature, the mode II interlaminar fracture toughness (G_{IIC}) of the nano-modified specimen was ~4 times higher than the virgin specimen (non-modified) (3.12 kJ/m^2 vs 0.81 kJ/m^2). The results showed that G_{IIC} of the virgin specimen was independent of temperature. However, in the case of the nano-modified specimen, although the G_{IIC} did not change from room temperature to 100 °C (3.12 kJ/m^2 vs 3.09 kJ/m^2), by further increasing temperature to 125 °C and 160 °C, G_{IIC} dropped by 34% and 43% respectively (2.05 kJ/m^2 and 1.77 kJ/m^2 respectively). 3D surface scans and Scanning Electron Microscopy (SEM) images of the fracture surface revealed three reasons for decreasing the toughening capability of the PA66 nanofibers at high temperatures: a) the crack crosses the nano-layer less at high temperatures, b) the dominant damage mechanism at low temperature is "cohesive failure", the damage propagation within the nanolayer, while at higher temperatures "adhesive failure", the debonding of the nanolayer from carbon fibers, plays a critical role in the fracture, and c) severe plastic deformation of nanofibers at high temperatures.

1. Introduction

Fiber Reinforced Polymer (FRP) composites are characterized by high specific in-plane mechanical properties. However, their relatively poor out-of-plane properties, specifically interlaminar fracture toughness, have limited utilizing the full potential that these materials can offer. Different methods have been proposed in the literature for increasing the interlaminar fracture toughness, such as matrix modification with nanoparticles [1–4], tufting [5–7], z-pinning [8–10], stitching [11–13], and 3D weaving [14,15]. However, some issues have restricted employing those toughening methods in real industrial applications. For example, although modification of resin with nanoparticles could enhance both in-plane and out-of-plane mechanical properties of composites, there are some challenges in producing these materials, such as making a uniform dispersion of nanoparticles in the resin and the control of the viscosity and temperature of the nano-modified resin during the sonication of nanoparticles [16]. In the case of other toughening methods, such as z-pinning and 3D weaving, although the out-of-plane properties can be improved significantly, they result in the reduction of in-plane mechanical properties of the laminate [17,18]. It has been reported that the z-pinning reduces in-plane modulus and strength because of the fiber damage at z-pins locations and the formation of resin-rich regions around z-pins [19]. In the case of 3D woven composites, the increase of yarn crimp reduces in-plane stiffness [20,21].

Interleaving composite plies by thermoplastic electrospun nanofibers mat is another toughening method that has attracted much attention lately [22–24]. In this method, the thermoplastic nanofibers mat with a thickness of order of micrometers, produced by the electrospinning process, is inserted between the composite plies during the laminating

* Corresponding author.
E-mail address: m.saeedifar@tudelft.nl (M. Saeedifar).

https://doi.org/10.1016/j.compscitech.2021.109061
Received 8 March 2021; Received in revised form 24 June 2021; Accepted 19 September 2021
Available online 25 September 2021

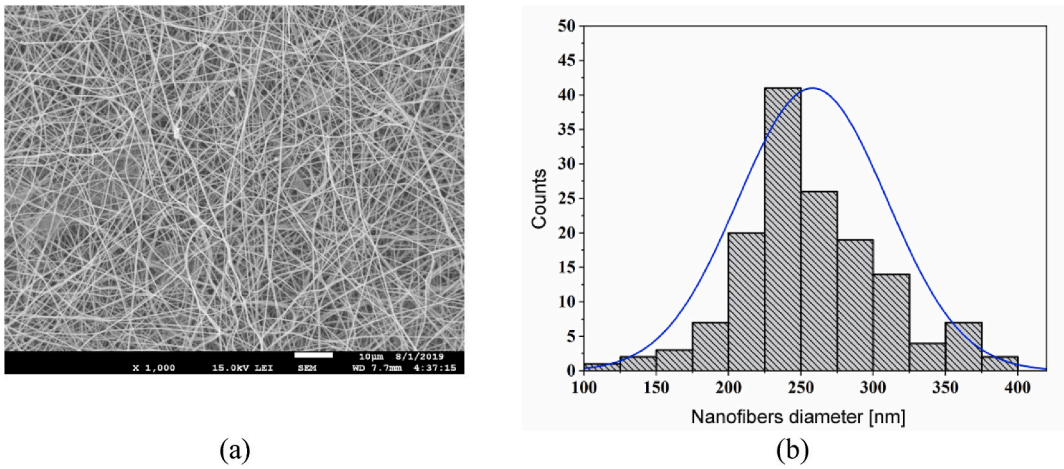

Fig. 1. a) The SEM image of the produced PA66 nanofibers, and b) diameter distribution of the nanofibers.

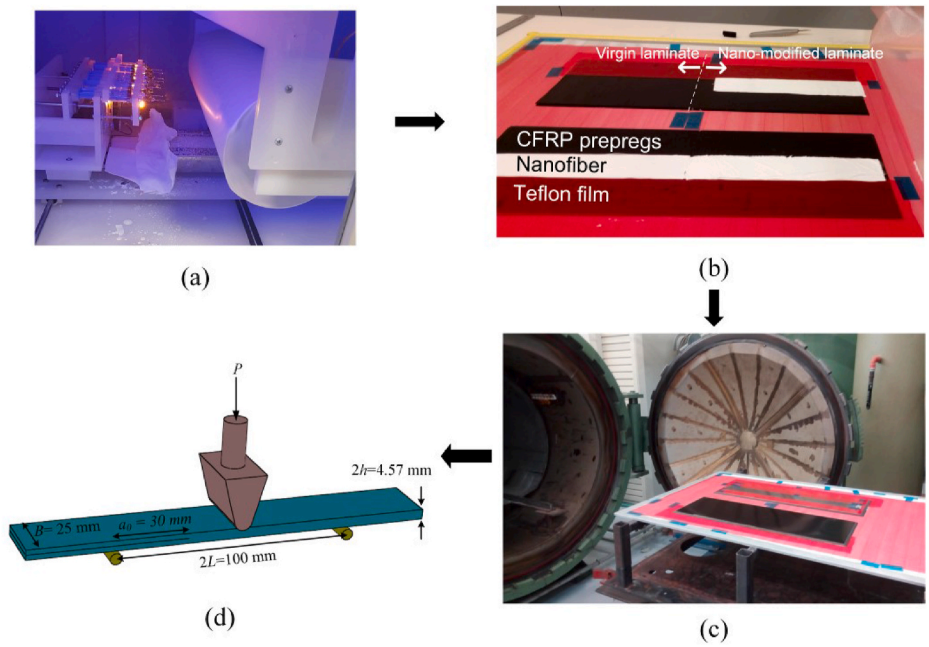

Fig. 2. The ENF specimen manufacturing process; a) electrospinning, b) laminating, c) curing in the autoclave, and d) 3-Point Bending (3PB) test configurations.

process and it is cured with the laminate. The toughening mechanisms of these nanofibers are different and depend on the nanofiber material, electrospinning process parameters, curing temperature of the interleaved laminate, etc. For example, bridging is the main toughening mechanism of Polyamide 66 (PA66) [25,26], while the toughening mechanism of polysulfone is the phase separation [27]. In the case of Polycaprolactone (PCL), the toughening mechanism depends on the curing temperature of the interleaved laminate. If the curing temperature is lower than the glass transition temperature (T_g) of PCL, the nanofibers bridging is the main toughening mechanism, while if the curing temperature is higher than the T_g, the phase separation will be the dominant toughening mechanism [24].

Among electrospun nanofibers, PA66 has shown good potential for toughening of laminated composites. Saghafi et al. [28] reported 62% and 109% increase in the mode I and mode II interlaminar fracture toughness (G_{IC} and G_{IIC}) of PA66-interleaved glass/epoxy laminated composites respectively. The difference in the toughening capability under mode I and mode II loading conditions refers to the fact that in the case of mode I loading conditions, nanofibers peel off is the dominant damage mechanism. Whereas in the case of mode II loading conditions, the nanofibers are appropriately bridged and consequently, the dominant damage mode is the fracture of the bridged nanofibers due to the applied shear stress [29]. Palazzetti et al. [30] studied the effect of nanomat thickness on the toughening capability of electrospun PA66 nanofibers. The results showed that for the mode I test, the lower the nanomat thickness, the better the toughening, while the mode II toughness was independent of the nanomat thickness. Brugo et al. [31,32] reported an increase of 130% in G_{IC} of the plain-weave carbon/-epoxy laminates interleaved by PA66 nanofibers.

In all aforementioned studies, the toughening capability of electrospun PA66 nanofibers has been investigated at room temperature. However, the interleaved composite structure may operate in environmental conditions where high temperatures, above 50 °C, exist. For a transport aircraft, minimum and maximum service temperatures are usually considered −54 °C and 71 °C [33], however higher temperatures have been also reported in the literature. For example, due to operation or environmental conditions, some components may be subjected to temperatures as high as 90–110 °C [33,34]. In addition, it is reported

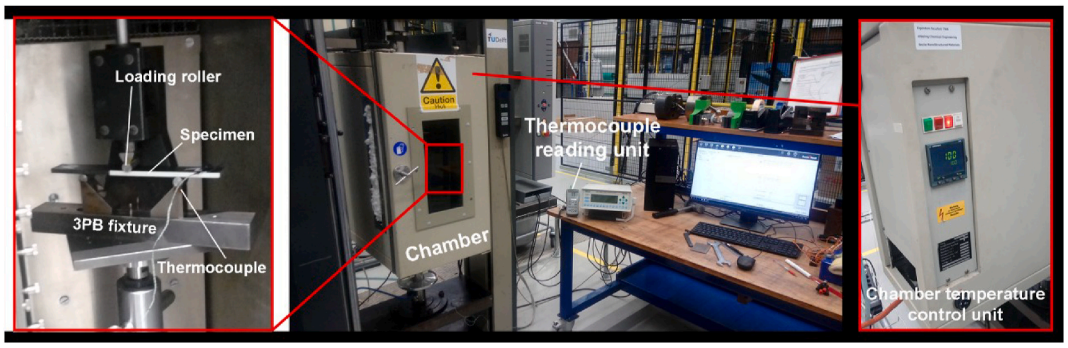

Fig. 3. The high-temperature mode II fracture test setup.

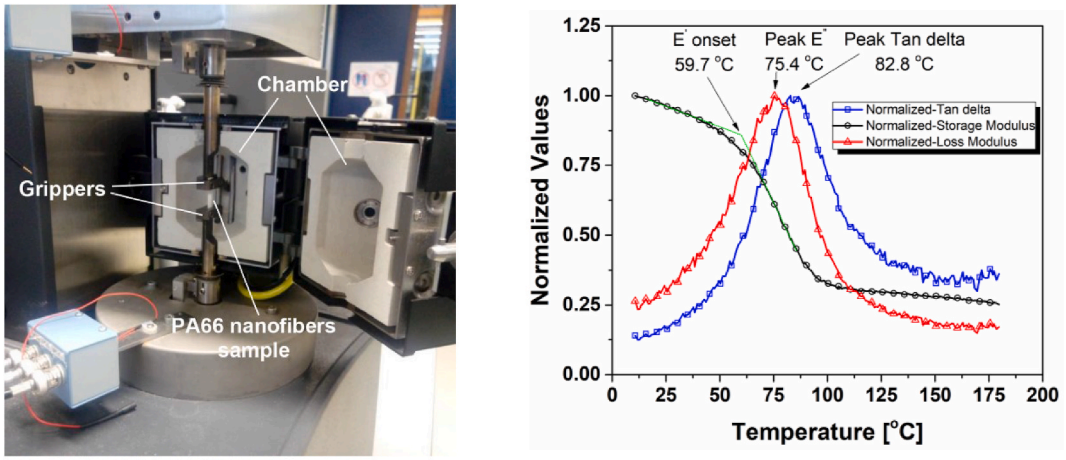

Fig. 4. a) The experimental setup, and b) the results of the DMA test of electrospun PA66 nanofibers.

that for some special cases, such as supersonic flights, the maximum temperature might raise up to 130–135 °C [35,36]. Higher temperatures up to 175 °C have been also investigated in the literature for carbon/-epoxy composites [37]. Taking into account relatively low T_g of electrospun PA66 nanofibers (T_g~60–80 °C), it is essential to evaluate the toughening capability of electrospun PA66 nanofibers at temperatures higher than its T_g. This research question is addressed in the present study by means of mechanical results, 3D scan fractography and Scanning Electron Microscopy (SEM) method.

2. Materials and manufacturing

2.1. PA66 nanofibers manufacturing process

The PA66 nanofibers were produced by the electrospinning process, in which by applying an electric field between the nozzles and the collector, a very narrow jet of the polymer solution gets out from the nozzle tip and are deposited randomly on a rotary collector. For producing the nanofibers, a solution of 20% w/v PA66 pellets dissolved in 30/70 v/v of formic acid and 2.2.2-Trifluoroethanol was used. The electrospinning process parameters are as follows: nozzle to collector distance: 12 cm, the rotational speed of the collector: 100 rpm, and the applied electrical voltage: 28 kV. SEM images of the produced PA66 nanofibers and the distribution of the nanofibers' diameter are illustrated in Fig. 1. The surface density and thickness of the produced nanofibers mat are 7.5 gr/m^2 and ~50 μm respectively.

2.2. Laminating process

The composite specimens were fabricated from 24 layers of unidirectional AS4/8552 carbon/epoxy prepregs, supplied by Hexcel Corporation. The nominal fiber volume is 57.42%, and the Tg of the epoxy resin after curing is 200 °C. The initial pre-crack was created by inserting a Teflon film with a thickness of ~13 μm between the 12th and 13th prepreg layers. The PA66 nanofibers mat was first dried in a vacuum oven for 2 h and it was then inserted at the front of the Teflon film. After laminating all the prepreg layers, the panel was sealed by a vacuum bag and cured in an autoclave according to the curing cycle provided by the prepreg's manufacturer [38]. The heating rate was selected as the minimum allowable value (1 °C/min) to give the epoxy resin enough time to infiltrate into the PA66 nanofibrous structure. Afterward, the composite panel was cut into the standard End-Notched Flexure (ENF) specimen size by means of a sharp rotary diamond blade. The final dimensions of ENF specimens were 170 × 25 × 4.5 mm^3 with an initial crack length of 70 mm. Because all virgin and nanomodified specimens were cut out of the same large composite panel, the thickness variation was not significant (a thickness of 4.5 ± 0.1 mm). The manufacturing process of the specimens and a schematic of the ENF test fixture are illustrated in Fig. 2.

3. Experimental methods

The mode II interlaminar fracture toughness test was conducted according to the ASTM D7905 standard [39]. The ENF specimen was subjected to a 3PB load, in which the initial crack length was 30 mm. The bottom support span was 100 mm and the upper roller applied load

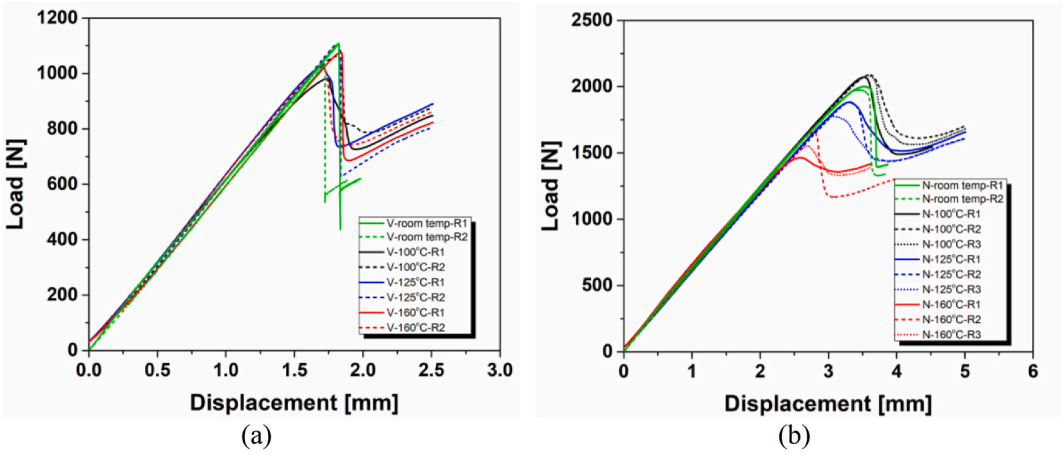

Fig. 5. The load-displacement curve of the a) virgin, and b) nano-modified ENF specimens at different temperatures (R indicates the test repetition number).

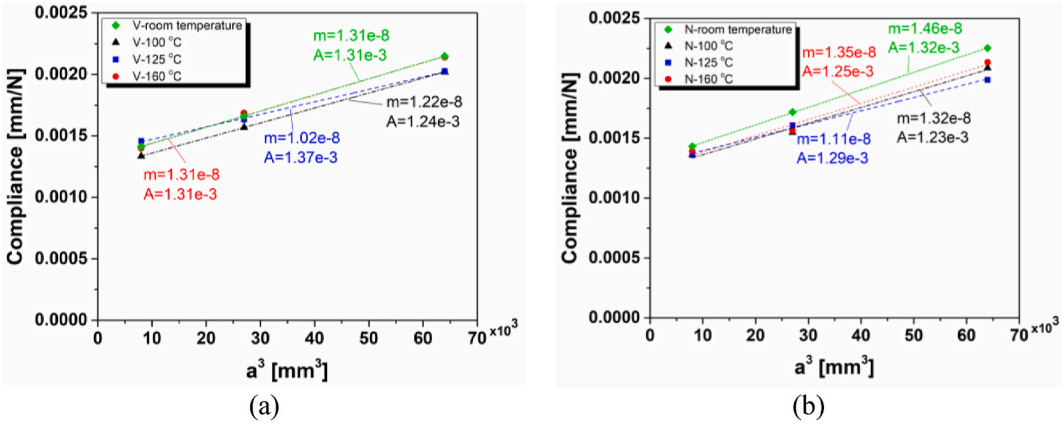

Fig. 6. Compliance calibration test of the a) virgin, and b) nano-modified ENF specimens.

Table 1
The mode II interlaminar fracture toughness of the virgin and nano-modified specimens at different temperatures.

Specimen	Temperature (°C)	δ_{cr} (mm)	P_{cr} (N)	G_{IIC} (kJ/m^2)
Virgin	Room temp.	1.77 ± 0.07	1069.91 ± 54.70	0.81 ± 0.08
Virgin	100 °C	1.77 ± 0.04	1020.76 ± 57.63	0.69 ± 0.08
Virgin	125 °C	1.76 ± 0.08	1066.21 ± 60.73	0.63 ± 0.07
Virgin	160 °C	1.77 ± 0.10	1047.36 ± 40.64	0.78 ± 0.06
Nano-modified	Room temp.	3.51 ± 0.04	1938.33 ± 19.65	3.12 ± 0.06
Nano-modified	100 °C	3.57 ± 0.04	2081.35 ± 9.63	3.09 ± 0.03
Nano-modified	125 °C	3.23 ± 0.12	1848.04 ± 62.63	2.05 ± 0.14
Nano-modified	160 °C	2.69 ± 0.10	1557.94 ± 96.26	1.77 ± 0.22

to the specimen at the middle of the support span. Before conducting the main fracture test, two preliminary tests with an initial crack length of 20 mm and 40 mm were performed to obtain the compliance calibration parameters, required by the standard for accurate calculation of G_{IIC}. During the calibration tests, when the load reached 500 N (less than half of the maximum load of the main test), the test was stopped for preventing crack propagation in the preliminary tests.

Based on the Dynamic mechanical analysis (DMA) test of electrospun PA66 nanofibers, which will be presented in section 4.1, the T_g of the produced nanofibers was in a range of ~60–80 °C. Based on the obtained T_g, the mode II fracture tests were performed in four temperature levels: room temperature (~25 °C), 100 °C, 125 °C, and 160 °C, in which the first temperature level, was much lower than the T_g temperature of the nanofibers, while the three other temperatures were higher than the T_g. The highest temperature, i.e., 160 °C, was selected close to the curing temperature of the prepregs (180 °C). In order to perform the high-temperature mode II tests, ENF specimens were first kept in an oven for 6 h at the same temperature at which they would be loaded, i.e., 100 °C, 125 °C, and 160 °C. Afterward, each test specimen was moved quickly to a Zwick 20 kN universal tension/compression machine equipped with a temperature chamber that had been already heated up to the test's temperature. The specimen was rapidly placed on the 3PB test fixture and a thermocouple wire was attached to its surface to indicate the temperature on the surface of the specimen. Then, the chamber's door was closed and enough time was given to the whole system until all the chamber, 3PB fixture and the ENF specimen reached the equilibrium state at the test's temperature. Finally, the compliance calibration and the main fracture tests were performed (see Fig. 3).

4. Results and discussion

4.1. Dynamic mechanical analysis (DMA) results

For determining the T_g of PA66 nanofibers, the DMA test was performed on a small strip of electrospun PA66 nanofibers sheet in

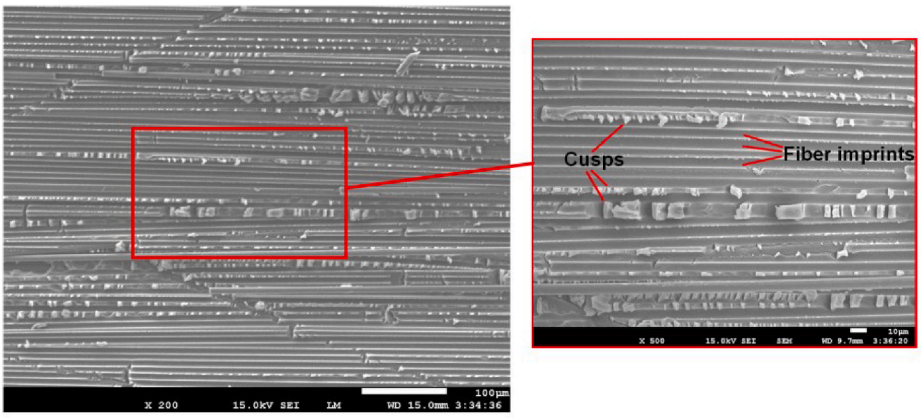

(a)

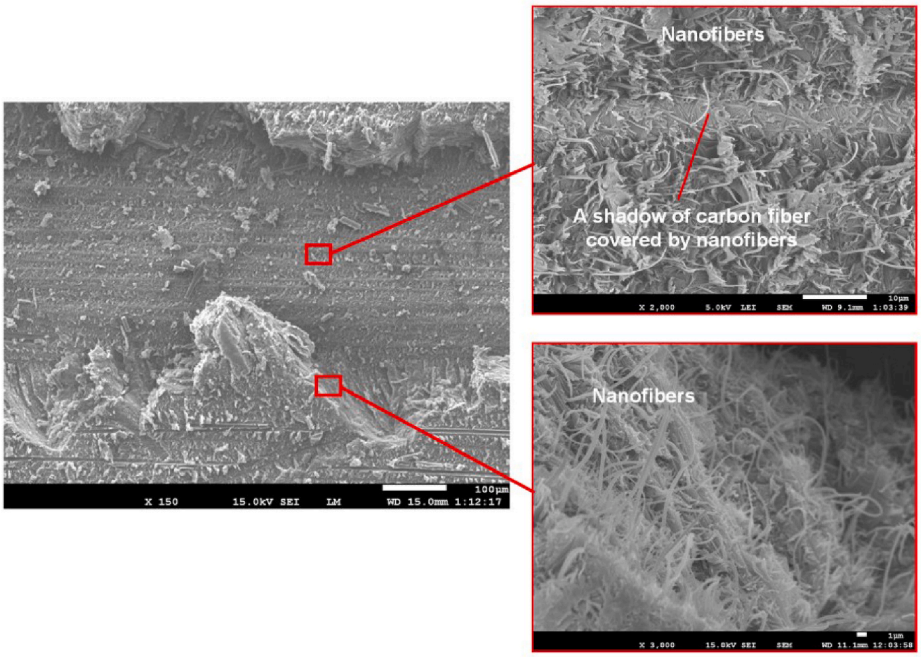

(b)

Fig. 7. The fracture surface of a) virgin, and b) nano-modified specimens.

dimensions of 30 × 9 mm^2. As illustrated in Fig. 4(a), the sample was subjected to a sinusoidal tensile load by means of two miniature grips of the DMA machine. The tensile load was applied to the sample with a frequency of 1 Hz in a temperature range of 10°C–180 °C with a temperature ramp of 3 °C/min. The normalized storage modulus (E′), loss modulus (E″) and tan delta (the ratio of E"/E′) curves are depicted in Fig. 4(b). The E′ and E″ indicate the stored energy, i.e., elastic response, and the dissipated energy as heat, i.e., viscous response, of the material respectively. According to the literature, the T_g can be determined in three ways [40]: initiation of the drop in the storage modulus (E′), the peak of the loss modulus (E″), and the peak of the tan delta. The E′ corresponds to short-range relaxations in polymer chains which reduce the resistance of the material against deformation. However, because identification of this point might be challenging, especially for polymers with a broad distribution of molecular weights, the peak of E″ can also be reported as the T_g (which occurs after the onset of the E′ drop). In addition, in many cases, the peak of the tan delta has been considered as the T_g [40]. Therefore, a range from 59.7 °C to 82.8 °C can be considered for the T_g of electrospun PA66 nanofibers. Therefore, based on the obtained T_g, the ENF tests were performed at the four temperatures mentioned in section 3.

4.2. Mechanical results

The load-displacement curves of the ENF tests at different temperature levels are depicted in Fig. 5. The stiffness of virgin and nano-modified specimens is not affected by the temperature variations. However, in the case of the maximum load, although the virgin specimens do not show a significant change, the maximum load of the nano-modified specimens is significantly dropped by increasing temperature. The G_{IIC} of ENF specimens is calculated as follows [39]:

$$G_{IIC} = \frac{3mP_{cr}^2 a_0^2}{2B} \tag{1}$$

$$C = A + ma^3 \tag{2}$$

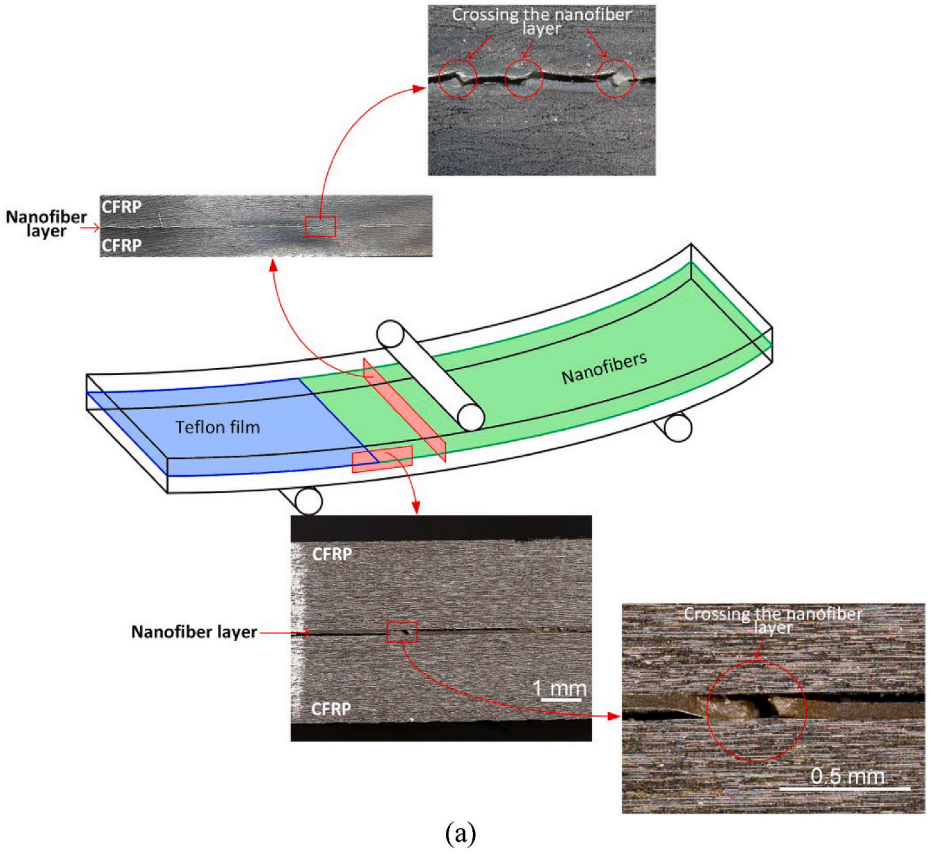

Fig. 8. a) Nano-layer crossing in both longitudinal and transverse directions, and b) the distribution of nanofibers between two carbon fabric plies.

where P_{cr} is the critical load corresponding to the delamination growth, which is considered as the maximum load in the load-displacement curve, a_0 denotes the initial delamination length, 30 mm, B indicates the width of the specimen, 25 mm, C is compliance, and m and A are the compliance calibration coefficients. In order to calculate the m factor, the compliance value (inverse of the slope of the load-displacement curve at the initial linear elastic region) should be calculated by conducting the preliminary compliance calibration tests with an initial delamination length of 20, 40 and 30 mm. Then, these compliance values (C) are plotted against the cube of corresponding initial delamination lengths (a^3). By fitting a linear equation to the datapoints, compliance calibration coefficients (A and m) are calculated by Eq. (2). The fitted linear equations, the compliance calibration coefficients and the G_{IIC} values for virgin and nano-modified specimens at different temperatures are presented in Fig. 6 and Table 1. As reported in Table 1, at room temperature, G_{IIC} of the nano-modified specimen is ~4 times higher than the virgin specimen that indicates the fact that applying the nanomat significantly increased the G_{IIC}. By increasing the temperature, G_{IIC} of the virgin specimens has not been affected significantly which shows the fact that the resistance of the virgin specimen is independent of the temperature up to temperatures close to its curing temperature. In the case of nano-modified specimens, the G_{IIC} does not change from room temperature to 100 °C (3.12 vs 3.09 kJ/m^2), but by further

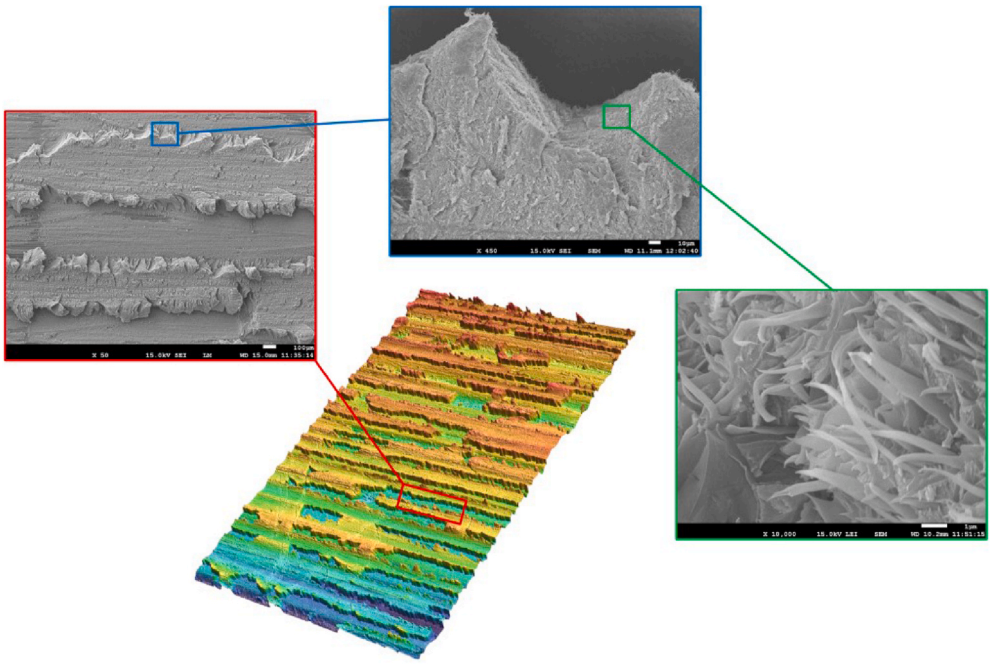

Fig. 9. 3D scan of the fracture surface of the nano-modified specimen.

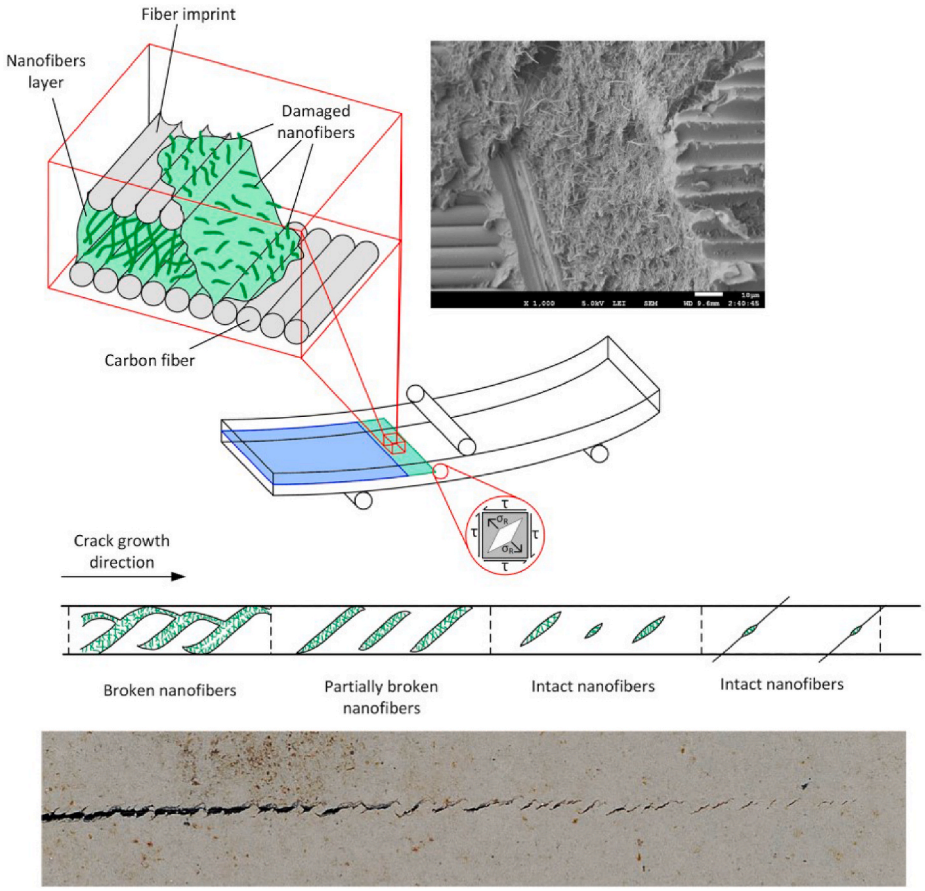

Fig. 10. The toughening mechanisms of the PA66 nanofibers in mode II loading conditions.

increasing temperature to 125 °C, G_{IIC} drops from 3.09 kJ/m^2 to 2.05 kJ/m^2. In addition, when the temperature is increased to 160 °C, G_{IIC} decreases to 1.77 kJ/m^2. Although the G_{IIC} of the nano-modified specimen is still 2.3 times the virgin specimen at the highest temperature, the results showed that the mode II toughening capability of PA66 nanofibers significantly depends on the temperature at temperatures higher than 100 °C.

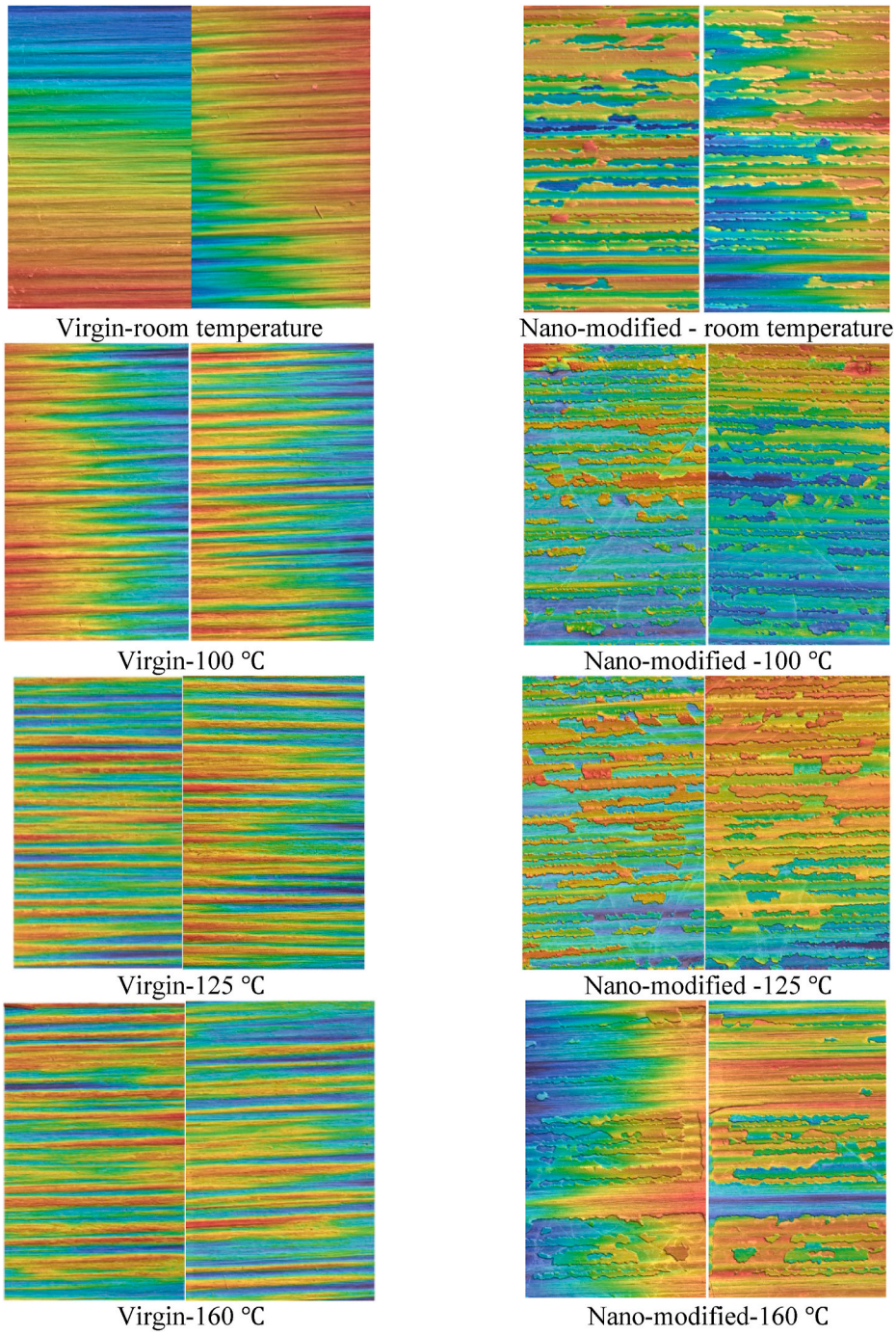

Fig. 11. The 3D images of the fracture surface of the specimens.

4.3. SEM and fractography results

The toughening mechanisms of electrospun PA66 nanofibers are explored by investigating the fractographic features on the damaged surface of the virgin and nano-modified specimens using Scanning Electron Microscope (SEM) and the wide-area 3D surface scanner, VR-5000 from KEYENCE Corporation. As depicted in Fig. 7, the dominant damage mechanisms in SEM images of the virgin specimens are matrix cracking, in the form of cusps, and fiber/matrix debonding, observed in the form of fiber imprints. Cusps are microcracks created normal to the maximum principal stress at the intermatrix spacing between the carbon fibers [41]. A closer view of the fracture surface reveals a clean and smooth surface of fiber imprints that indicates weak adhesion between carbon fibers and matrix. However, the fracture surface of the nano-modified specimens differs completely from the virgin specimens and it is almost covered by a thin layer of nanofibers that suspended the formation of cusps and fiber imprints. In the case of the virgin specimen, the main damage mechanism is carbon fibers peeling results in the separation of carbon fibers from the resin matrix which is appeared as fiber imprints on the fracture surface. However, in the case of the nanomodified specimen, the dominant damage mode is the bridging of nanofibers. Therefore, the fracture surface is usually covered by a layer of nanofiber,s and carbon fibers are embedded in the nanofibers mat. As stated in Fig. 7(b), a large number of broken nanofibers on the fracture surface indicate the effective bridging of the nanofibers during the delamination growth.

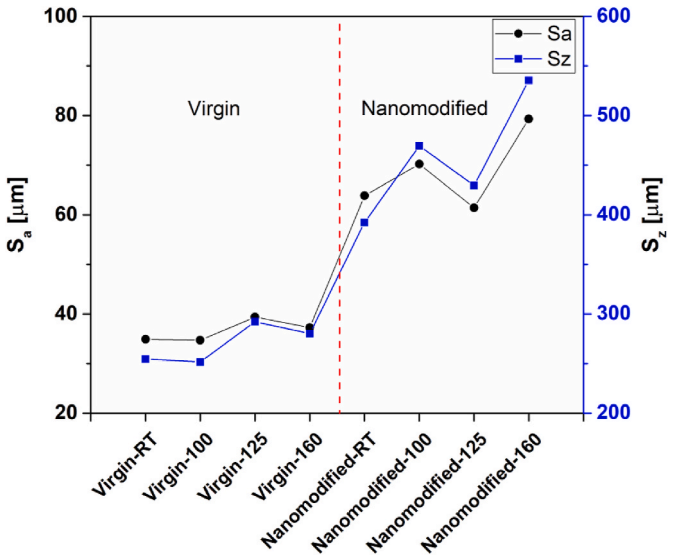

Fig. 12. The Surface roughness of the fracture surface of ENF specimens.

As depicted in Fig. 7(b), the crack has crossed the nano-layer during propagation. Crossing the nano-layer increases the fracture toughness by involving the nanofibers located on the fracture ramp in the bridging process [29,42]. For quantifying the effect of the nano-layer crossing on the toughening capability, the nano-layer crossing is depicted in the front and lateral views of the nano-modified specimen in Fig. 8(a). As it is clear, the crack crossed the nanofiber layer in both longitudinal and transverse directions. From the lateral view, it is seen that the delamination initially propagated at the bottom of the nano-layer, and after a few millimeters, it crossed the nano-layer and jumped to the top of the nano-layer. This phenomenon happened several times along the crack growth direction. Therefore, the delamination growth can be considered as a combination of the interfacial debonding, i.e., adhesive failure, and interlaminar nano-layer crossing. The front view of the specimen also reveals several nano-layer crossing across the specimen's width. Therefore, the main toughening mechanism of PA66 nanofibers is the bridging of nanofibers in two forms: 1) increasing the bonding strength of the interlaminar resin-rich region to the adjacent composite prepregs (improving resistance against the adhesive failure), and 2) increasing the toughness of the interlaminar resin-rich region (improving resistance against the nano-layer crossing). The distribution of nanofibers between two carbon fabric plies is depicted in Fig. 8(b). A 3D scan of the fracture surface of the nano-modified specimen can give a better understanding of the interlaminar nano-layer crossing (see Fig. 9). The 3D scan shows many separated nanomat islands on the fracture surface at which many nanofibers bridging occurred at the boundaries of these islands (fracture ramps).

Besides the aforementioned mechanisms, the nanofibers postpone the delamination growth with an additional mechanism. In order to find out this mechanism, the process of the shear delamination growth in laminated composites should be clarified firstly. As depicted in Fig. 10, once the ENF specimen is loaded under shear loading, the shear stress at the crack tip introduces tensile traction at an angle of 45° to the crack plane that result in the formation of inclined matrix microcracks at the crack tip region. By increasing the load, these microcracks elongate at an angle of 45°. The macroscopic delamination growth occurs once these microcracks interconnect together. The nanofibers postpone the initiation of matrix microcracks by toughening the interlaminar resin-rich region and also reduce the evolution rate of the microcracks by bridging between the surfaces of the microcracks.

After the declaration of the toughening mechanisms of the PA66 nanofibers, the reasons for decreasing the toughening capability of the nanofibers at high temperatures can be discussed. The 3D scan images of the virgin and nano-modified specimens are illustrated in Fig. 11. For each condition, both top and bottom fracture surfaces are shown next to each other. The surface of the virgin specimens, irrespective of the test temperature, is much smoother than the nano-modified ones. A large waviness is observed on the fracture surface of the virgin specimens, as a result of the waviness of the fiber yarn patterns of the prepreg. While, in the case of nano-modified specimens, the fracture surface is obviously rough and the traces of the nanofibers layer on both top and bottom surfaces are clearly visible. Surface roughness parameters of the arithmetical mean height (S_a) and the maximum height (S_Z) of the fracture surface of ENF specimens are depicted in Fig. 12. As it is clear, the surface roughness of nanomodified specimens is more than two times of virgin specimens. By comparing the fracture surface of the nano-modified specimens at different temperatures, it is revealed that for temperatures of 25 °C, 100 °C and 125 °C, many isolated/separated nano-layer islands are visible, while by increasing the temperature to 160 °C, the number of isolated islands decreases and there are a couple of large pieces of nano-layer on the fracture surface. Therefore, the nano-layer crossing is reduced which consequently decreases the potential toughening of the nanofibers placed on the nanomat fracture ramps. This fact reveals that at the highest temperature (160 °C), the crack mainly propagated at the interface of nanomat and the composite ply, and the main toughening mechanism is the bridging of the nanofibers located on the composite ply surface.

The SEM images of the fracture surface of specimens give a better understanding of the fracture process at different temperatures. As depicted in Fig. 13, at room temperature and 100 °C, the fracture surface of the nano-modified specimen is almost covered by a thin layer of nanofibers. This indicates the good adhesion of the nanofibers to the carbon fibers. The amount of naked carbon fibers in these two temperatures is negligible that reveals the fact that the delamination mainly propagated in the "cohesive failure" mode. While, by increasing temperature to 125 °C and 160 °C, naked carbon fibers on the fracture surface increase that indicates the fact that besides the cohesive failure, the adhesive failure plays a critical role in the delamination growth. The adhesive failure is an indication of weak bonding between the nanofibers and the composite plies at high temperatures, i.e., 125 °C and 160 °C. Moreover, looking at the shape of the damaged nanofibers reveals a valuable fact. The high-magnified images of the fracture surface of nano-modified specimens at room temperature and 100 °C indicate a lot of rod-shaped damaged nanofibers, while by increasing the temperature to 125 °C, the end of some of the damaged nanofibers, which were oriented along the direction of the applied shear stress, became needle-shaped that reveals significant plastic deformation of those nanofibers. In the case of 160 °C, damaged nanofibers parallel to the shear stress direction have been flatten because of severe plastic deformation at this temperature. Regarding virgin specimens, SEM images show that the dominant damage mechanisms are fiber/matrix debonding and matrix cracking and no significant difference is distinguished among different temperatures. This is consistent with similarities observed among the 3D scans and the constant G_{IIC} of the virgin specimens at different temperatures.

In conclusion, the main reasons for decreasing the fracture toughness values of the nano-modified specimens at high temperatures are summarized hereafter:

1) Decreasing the nano-layer crossing at the highest temperature (160 °C)
2) The dominant damage mode of the delamination growth at room temperature and 100 °C is the cohesive failure, while by increasing the temperature to 125 °C and 160 °C, besides the cohesive failure, the adhesive failure plays a critical role in the crack growth.
3) Severe plastic deformation of nanofibers at 125 °C and 160 °C.

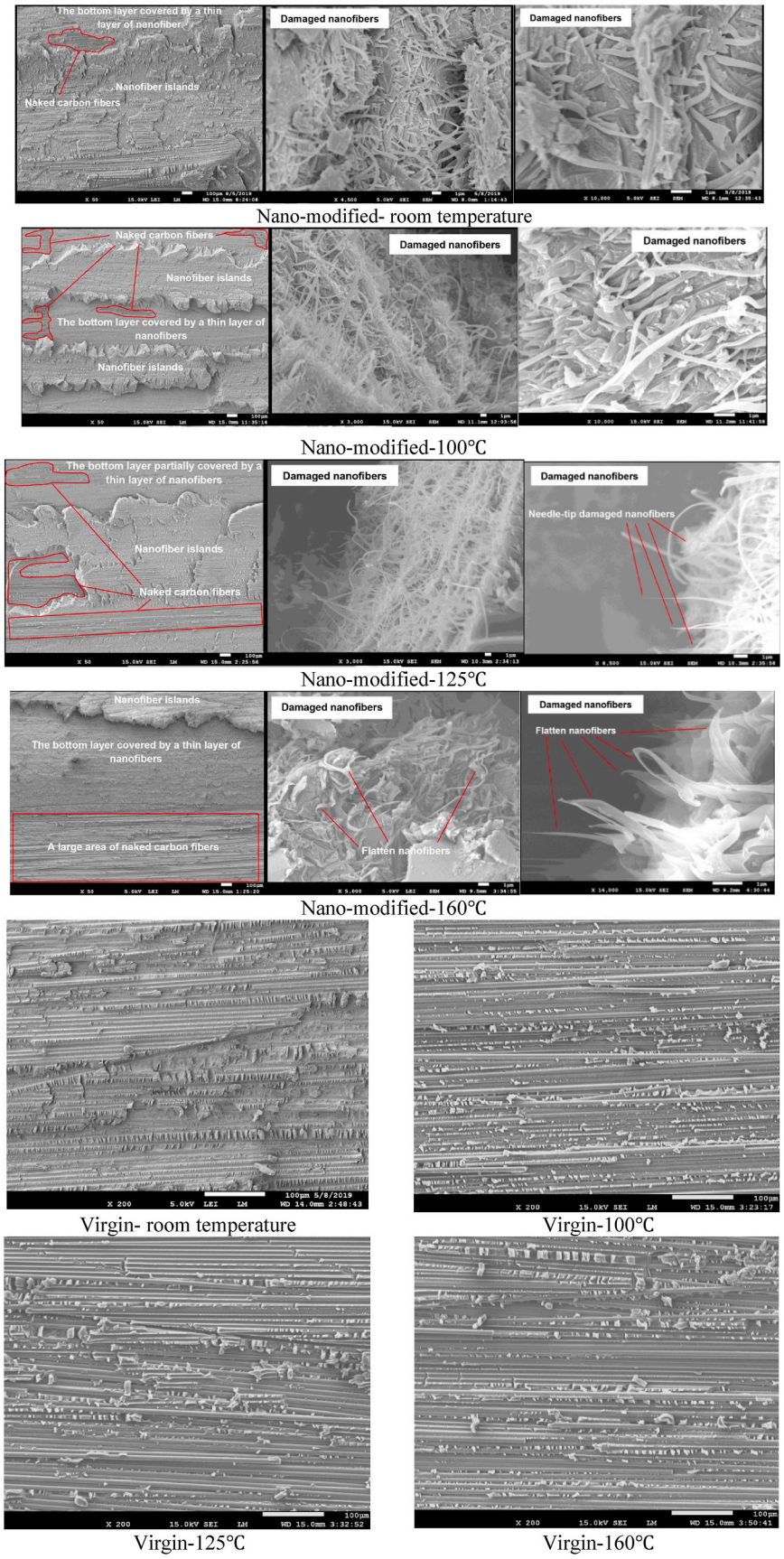

Fig. 13. The SEM images of the nano-modified and virgin specimens.

5. Conclusion

The toughening capability of electrospun PA66 nanofibers for carbon/epoxy laminates at elevated temperatures was evaluated. The quasi-static mode II interlaminar fracture toughness tests of the End-Notched Flexure (ENF) carbon/epoxy specimens revealed that the mode II interlaminar fracture toughness (G_{IIC}) of nano-modified specimen at room temperature and 100 °C is ~4 times higher than the virgin specimen (non-modified). The G_{IIC} of the virgin specimen was not affected by increasing the temperature, while in the case of nano-modified specimen, it dropped by 34% and 43% by increasing the temperature up to 125 °C and 160 °C, respectively. The 3D scan and SEM images revealed that this reduction in the fracture toughness is related to three factors: 1) decreasing the nano-layer crossing at high temperatures, 2) the dominant damage mode at lower temperatures is the cohesive failure, while by increasing the temperature to 125 °C and 160 °C, the adhesive failure is involved in the fracture process as well, and 3) severe plastic deformation of nanofibers at 125 °C and 160 °C.

Funding

No funding resources.

Data availability

The raw/processed data required to reproduce these findings cannot be shared at this time as the data also forms part of an ongoing study.

Credit authorship contribution statement

Milad Saeedifar: Conceptualization, Methodology, Investigation, Formal analysis, Writing - original draft, Writing - review & editing.

Hamed Saghafi: Conceptualization, Investigation, Writing - original draft, Writing - review & editing.

Reza Mohammadi: Conceptualization, Formal analysis, Writing - original draft.

Dimitrios Zarouchas: Supervision, Writing - original draft, Writing - review & editing.

Declaration of competing interest

The authors declare that they have no known competing financial interests or personal relationships that could have appeared to influence the work reported in this paper.

References

[1] Y. Tang, L. Ye, Z. Zhang, K. Friedrich, Interlaminar fracture toughness and CAI strength of fibre-reinforced composites with nanoparticles – a review, Compos. Sci. Technol. 86 (2013) 26–37.
[2] A.F. Yee, in: N.J. Johnston (Ed.), Modifying Matrix Materials for Tougher Composites, ASTM International, West Conshohocken, PA, 1987, pp. 383–396.
[3] S. Sprenger, M.H. Kothmann, V. Altstaedt, Carbon fiber-reinforced composites using an epoxy resin matrix modified with reactive liquid rubber and silica nanoparticles, Compos. Sci. Technol. 105 (2014) 86–95.
[4] M.H. Nguyen, P. Davidson, A.M. Waas, Particle-toughened interlayers enhance mechanical response of composite laminates, Compos. Sci. Technol. 182 (2019) 107761.
[5] M. Colin de Verdiere, A.K. Pickett, A.A. Skordos, V. Witzel, Evaluation of the mechanical and damage behaviour of tufted non crimped fabric composites using full field measurements, Compos. Sci. Technol. 69 (2) (2009) 131–138.
[6] A.T. Martins, Z. Aboura, W. Harizi, A. Laksimi, K. Khellil, Analysis of the impact and compression after impact behavior of tufted laminated composites, Compos. Struct. 184 (2018) 352–361.
[7] K.K. Verma, S.R. Viswamurthy, K.M. Gaddikeri, S. Ramesh, S. Kumar, S. Bose, Tufting thread and density controls the mode-I fracture toughness in carbon/epoxy composite, Compos. Struct. 261 (2021) 113272.
[8] A.P. Mouritz, Review of z-pinned laminates and sandwich composites, Compos. Appl. Sci. Manuf. 139 (2020) 106128.
[9] A.R. Ravindran, R.B. Ladani, C.H. Wang, A.P. Mouritz, Hierarchical mode I and mode II interlaminar toughening of Z-pinned composites using 1D and 2D carbon nanofillers, Compos. Appl. Sci. Manuf. 124 (2019) 105470.
[10] R.B. Ladani, A.R. Ravindran, S. Wu, K. Pingkarawat, A.J. Kinloch, A.P. Mouritz, R. O. Ritchie, C.H. Wang, Multi-scale toughening of fibre composites using carbon nanofibres and z-pins, Compos. Sci. Technol. 131 (2016) 98–109.
[11] K. Pingkarawat, C.H. Wang, R.J. Varley, A.P. Mouritz, Effect of mendable polymer stitch density on the toughening and healing of delamination cracks in carbon–epoxy laminates, Compos. Appl. Sci. Manuf. 50 (2013) 22–30.
[12] H. Li, Y. Yu, X. Xu, T. Chen, W. Lu, Enhancing the fracture toughness of laminated composites through carbon nanotube belt stitching, Compos. Sci. Technol. 204 (2021) 108632.
[13] L. Amorim, A. Santos, J.P. Nunes, J.C. Viana, Bioinspired approaches for toughening of fibre reinforced polymer composites, Mater. Des. 199 (2021) 109336.
[14] M.N. Saleh, H.M. El-Dessouky, M. Saeedifar, S.T. De Freitas, R.J. Scaife, D. Zarouchas, Compression after multiple low velocity impacts of NCF, 2D and 3D woven composites, Compos. Appl. Sci. Manuf. 125 (2019) 105576.
[15] M. Saeedifar, M.N. Saleh, H.M. El-Dessouky, S. Teixeira De Freitas, D. Zarouchas, Damage assessment of NCF, 2D and 3D woven composites under compression after multiple-impact using acoustic emission, Compos. Appl. Sci. Manuf. 132 (2020) 105833.
[16] B. Bittmann, F. Haupert, A.K. Schlarb, Ultrasonic dispersion of inorganic nanoparticles in epoxy resin, Ultrason. Sonochem. 16 (5) (2009) 622–628.
[17] W. Zhou, T. Wente, D. Liu, X. Mao, D. Zeng, H. Torab, J. Dahl, X. Xiao, A comparative study of a quasi 3D woven composite with UD and 2D woven laminates, Compos. Appl. Sci. Manuf. 139 (2020) 106139.
[18] A.P. Mouritz, Review of z-pinned composite laminates, Compos. Appl. Sci. Manuf. 38 (12) (2007) 2383–2397.
[19] P. Chang, A.P. Mouritz, B.N. Cox, Properties and failure mechanisms of z-pinned laminates in monotonic and cyclic tension, Compos. Appl. Sci. Manuf. 37 (10) (2006) 1501–1513.
[20] F. Stig, S. Hallström, Effects of crimp and textile architecture on the stiffness and strength of composites with 3D reinforcement, Advances in Materials Science and Engineering 2019 (2019) 8439530.
[21] F. Stig, S. Hallström, Influence of crimp on 3D-woven fibre reinforced composites, Compos. Struct. 95 (2013) 114–122.
[22] R. Palazzetti, A. Zucchelli, Electrospun nanofibers as reinforcement for composite laminates materials – a review, Compos. Struct. 182 (2017) 711–727.
[23] G. Wang, D. Yu, A.D. Kelkar, L. Zhang, Electrospun nanofiber: emerging reinforcing filler in polymer matrix composite materials, Prog. Polym. Sci. 75 (2017) 73–107.
[24] H. Saghafi, M. Fotouhi, G. Minak, Improvement of the impact properties of composite laminates by means of nano-modification of the matrix—a review, Appl. Sci. 8 (12) (2018).
[25] R. Mohammadi, M. Ahmadi Najafabadi, H. Saghafi, M. Saeedifar, D. Zarouchas, A quantitative assessment of the damage mechanisms of CFRP laminates interleaved by PA66 electrospun nanofibers using acoustic emission, Compos. Struct. 258 (2021) 113395.
[26] O. İnal, M.Ç. Akbolat, C. Soutis, K.B. Katnam, Toughening mechanisms in cost-effective carbon-epoxy laminates with thermoplastic veils: mode-I and in-situ SEM fracture characterisation, International Journal of Lightweight Materials and Manufacture 4 (1) (2021) 50–61.
[27] G. Li, P. Li, Y. Yu, X. Jia, S. Zhang, X. Yang, S. Ryu, Novel carbon fiber/epoxy composite toughened by electrospun polysulfone nanofibers, Mater. Lett. 62 (3) (2008) 511–514.
[28] H. Saghafi, R. Palazzetti, A. Zucchelli, G. Minak, Influence of electrospun nanofibers on the interlaminar properties of unidirectional epoxy resin/glass fiber composite laminates, J. Reinforc. Plast. Compos. 34 (11) (2015) 907–914.
[29] L. Daelemans, S. van der Heijden, I. De Baere, H. Rahier, W. Van Paepegem, K. De Clerck, Damage-resistant composites using electrospun nanofibers: a multiscale Analysis of the toughening mechanisms, ACS Appl. Mater. Interfaces 8 (18) (2016) 11806–11818.
[30] R. Palazzetti, X. Yan, A. Zucchelli, Influence of geometrical features of electrospun nylon 6,6 interleave on the CFRP laminates mechanical properties, Polym. Compos. 35 (1) (2014) 137–150.
[31] T. Brugo, G. Minak, A. Zucchelli, X.T. Yan, J. Belcari, H. Saghafi, R. Palazzetti, Study on Mode I fatigue behaviour of Nylon 6,6 nanoreinforced CFRP laminates, Compos. Struct. 164 (2017) 51–57.
[32] T.M. Brugo, G. Minak, A. Zucchelli, H. Saghafi, M. Fotouhi, An investigation on the fatigue based delamination of woven carbon-epoxy composite laminates reinforced with Polyamide nanofibers, Procedia Engineering 109 (2015) 65–72.
[33] Composite Materials Handbook, Volume 3: Polymer Matrix Composites Materials Usage, Design, and Analysis, Department of Defense Handbook, USA, 2002.
[34] D. Petersen, R. Rolfes, R. Zimmermann, Thermo-mechanical design aspects for primary composite structures of large transport aircraft, Aero. Sci. Technol. 5 (2) (2001) 135–146.
[35] P. Mangalgiri, Polymer-matrix composites for high-temperature applications, Defence Sci. J. 55 (2) (2005) 175–193.
[36] J. Jedidi, F. Jacquemin, A. Vautrin, Accelerated hygrothermal cyclical tests for carbon/epoxy laminates, Compos. Appl. Sci. Manuf. 37 (4) (2006) 636–645.
[37] T.A. Collings, D.L. Mead, Effect of high temperature spikes on a carbon fibre-reinforced epoxy laminate, Composites 19 (1) (1988) 61–66.
[38] HexPly ® 8552 Epoxy matrix (180°C/356°F curing matrix), in: FTA 072e, Hexcel Composites Publication, 2013.
[39] ASTM Standard, D7905/D7905M–14, Standard Test Method for Determination of the Mode II Interlaminar Fracture Toughness of Unidirectional Fiber-Reinforced Polymer Matrix Composites, 2014.

[40] L. Lu, J. Pan, G. Li, Recyclable high-performance epoxy based on transesterification reaction, J. Mater. Chem. 5 (40) (2017) 21505–21513.
[41] E.S. Greenhalgh, Failure Analysis and Fractography of Polymer Composites, 2009.
[42] L. Daelemans, S. van der Heijden, I. De Baere, H. Rahier, W. Van Paepegem, K. De Clerck, Using aligned nanofibres for identifying the toughening micromechanisms in nanofibre interleaved laminates, Compos. Sci. Technol. 124 (2016) 17–26.